DAPI (4′,6-Diamidino-2-phenylindole) Binds Differently to DNA and RNA: Minor-Groove Binding at AT Sites and Intercalation at AU Sites†

Farial A. Tanious, James M. Veal, Henryk Buczak, Lynda S. Ratmeyer, and W. David Wilson*

Department of Chemistry and Laboratory for Chemical and Biological Sciences, Georgia State University, Atlanta, Georgia 30303

Received October 7, 1991; Revised Manuscript Received December 31, 1991

ABSTRACT: The interaction of DAPI and propidium with RNA (polyA·polyU) and corresponding DNA (polydA·polydT) sequences has been compared by spectroscopic, kinetic, viscometric, T_m, and molecular modeling methods. Spectral changes of propidium are similar on binding to the AT and AU sequences but are significantly different for binding of DAPI. Spectral changes for DAPI with the DNA sequence are consistent with the expected groove-binding mode. All spectral changes for complexes of propidium with RNA and DNA and for DAPI with RNA, however, are consistent with an intercalation binding mode. When complexed with RNA, for example, DAPI aromatic protons signals shift significantly upfield, and the DAPI UV–visible spectrum shows significantly larger changes than when complexed with DNA. Slopes of log k_d (dissociation rate constants) versus −log [Na^+] plots are similar for complexes of propidium with RNA and DNA and for the DAPI–RNA complex and are in the range expected for an intercalation complex. The slope for the DAPI–DNA complex, however, is much larger and is in the range expected for a groove-binding complex. Association kinetics results also support an intercalation binding mode for the DAPI–RNA complex. The viscosity of polyA·polyU solutions increases significantly on addition of both propidium and DAPI, again in agreement with an intercalation binding mode for both molecules with RNA. Molecular modeling studies completely support the experimental findings and indicate that DAPI forms a very favorable intercalation complex with RNA. DAPI also forms a very stable complex in the minor groove of AT sequences of DNA, but the stabilizing interactions are considerably reduced in the wide, shallow minor groove of RNA. Modeling studies, thus, indicate that DAPI interaction energetics are more favorable for minor-groove binding in AT sequences but are more favorable for intercalation in RNA.

The intense interest in DNA[1] as a receptor for anticancer agents has led to the discovery of many drugs which bind to DNA and exert their biological effects through a DNA complex (Waring, 1981; Wilson, 1990). Much less is known about RNA interactions, and there have been few detailed studies of the RNA binding modes of organic cations. Because of the serious diseases caused by RNA viruses, however, there is considerable interest in developing compounds that can interact with the RNA of these viruses and exert antiviral activity (Haseltine, 1989; Broder, 1989; Mitsuya et al., 1990; De-Clercq, 1990).

Two primary binding modes for organic cations with nucleic acids, intercalation and minor-groove interactions, have been identified. Typically, intercalators are planar aromatic cations and groove-binding ligands are unfused aromatic cations (Waring, 1981; Neidle & Abraham, 1984; Zimmer & Wahnert, 1986; Wilson, 1990); however, we have recently shown that some novel unfused aromatic compounds can bind with high affinity to DNA through an intercalation mode (Wilson et al., 1988, 1989a; Strekowski et al., 1987). This discovery indicates that factors other than ligand structure are critical to the binding mode and has led us to investigate the sequence dependence of the binding mode for classical minor groove binding agents such as DAPI (Wilson et al., 1989b, 1990a,b). We found with DAPI, for example, that it does have a very strong minor-groove binding mode in DNA AT sequences but that it binds by intercalation in GC or in mixed AT and GC DNA sequences (Wilson et al., 1989b, 1990a,b). At GC and mixed sequences the reduced depth and increased width of the minor groove compared to AT sequences (Saenger, 1984; Kopka et al., 1985) results in intercalation becoming more energetically favorable than minor groove binding. The DAPI binding strength in GC sequences is in the range typically observed for strong intercalators such as quinacrine and ethidium (Wilson et al., 1989b, 1990a,b).

In addition to binding with high affinity to DNA, DAPI has been shown to bind well to AU sequences in RNA, and it was proposed that, as with DNA AT sequences, the binding mode is through interactions in the RNA minor groove (Manzini et al., 1985). The minor and major grooves of A-form RNA duplexes, however, differ very significantly from those of B-form DNA. The grooves in RNA and DNA have different steric characteristics, different chemical characteristics due to features such as the 2′-OH group in the RNA minor groove, and different relative molecular electrostatic potentials (Saenger, 1984; Blackburn & Gait, 1990; Pullman & Pullman, 1981). Although the DNA and RNA grooves are quite different, X-ray analysis with intercalation complexes of dinucleotides and modeling studies with intercalators in segments of RNA and DNA have indicated that intercalation sites in both types of nucleic acid can be quite similar (Sheih et al., 1980; Berman et al., 1978; Islam & Neidle, 1984; Neidle, 1989; Veal & Wilson, 1991). Ethidium binding, for

† This work was supported by NIH Grant AI-27196.

[1] Abbreviations: RNA, ribonucleic acid; DNA, deoxyribonucleic acid; DAPI, 4′,6-diamidino-2-phenylindole; EDTA, ethylenediaminetetraacetic acid; MES, 2-(*N*-morpholino)ethanesulfonic acid; poly[d(A-T)]$_2$, poly[d(A-T)]·poly[d(A-T)]; poly[d(G-C)]$_2$, poly[d(G-C)]·poly[d(G-C)]; polyA·polyU, poly(rA)·poly(rU); polydA·polydT, poly(dA)·poly(dT); SDS, sodium dodecyl sulfate; NMR, nuclear magnetic resonance.

0006-2960/92/0431-3103$03.00/0

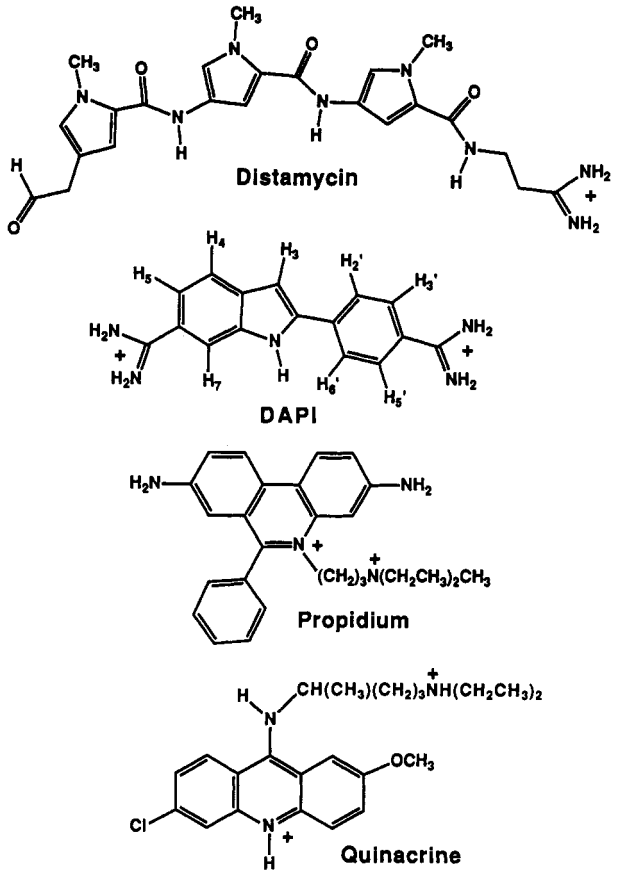

FIGURE 1: Structures of distamycin, DAPI, propidium, and quinacrine.

example, has been studied with both RNA and DNA polymers (Bresloff & Crothers, 1981; Babayan et al., 1987) and oligonucleotides (Nelson & Tinoco, 1984), and it binds strongly by intercalation to RNA and DNA.

These observations and the ability of DAPI to intercalate at GC and mixed GC/AT sequences in DNA suggested to us that DAPI might preferentially intercalate at AU sequences in RNA rather than bind in the minor groove as previously proposed. We report here a comparative investigation of the DAPI binding interactions with polyA·polyU and polydA·polydT. The results are compared to those of the classical dicationic intercalator propidium (Figure 1) under the same conditions, and to more limited results for the classical groove-binding molecule distamycin with the RNA polymer. Both experimental and theoretical results demonstrate that the most favorable DAPI binding mode with RNA is intercalation, and possible molecular models for the RNA intercalation and minor-groove binding sites are presented.

Materials and Methods

Materials. DAPI was obtained from Boehringer Mannheim Biochemicals, propidium was obtained from Calbiochem, and distamycin A was from Sigma. The structure and the purity of these compounds were confirmed by ^{1}H NMR and UV–visible spectroscopy. MES buffer at pH 6.2 contained 1×10^{-2} M 2-(*N*-morpholino)ethanesulfonic acid and 1×10^{-3} M EDTA. Sodium chloride was added to adjust the salt concentration of the buffers to the desired value. PolyA·polyU was purchased from Sigma, and polydA·polydT was from P-L Biochemicals. The polymers were prepared and dialyzed against MES buffer for the NMR study as previously described (Wilson et al., 1985a,c).

Viscometric Titrations. Viscometric titrations were conducted in Cannon-Ubbelohde semimicro-dilution viscometers in a constant temperature water bath as previously described for DNA (Jones et al., 1980).

Absorption and Fluorescence. Scans and extinction coefficients were determined as previously described (Wilson et al., 1985a; Wilson & Lopp 1979) with a Cary 2200 spectrophotometer. Fluorescence measurements were conducted on a SLM 8000C spectrofluorometer with excitation at 350 nm. DAPI solutions (6×10^{-6} M) in MES buffer with 0.1 M NaCl were scanned for emission spectra from 360 to 620 nm. Aliquots of DNA or RNA polymers stock solutions were added, and emission spectra were again obtained under the same conditions.

NMR. Spectra of solutions of DAPI were obtained as previously described (Chandrasekaran et al., 1986; Wilson et al., 1985c) in D_2O–MES buffer with 0.1 M NaCl at high temperatures (50–60 °C). The high temperature was used to obtain fast exchange and more narrow signals between free and bound DAPI as with DNA complexes (Wilson et al., 1989b, 1990a,b). A relatively low concentration (0.5 mM) of DAPI was necessary to minimize precipitation of the DAPI–RNA complex in the NMR experiments. Spectra were collected on Varian VXR 400 spectrometer at a spectral width of 4500 Hz, with a 1-s relaxation delay and TSP as an internal reference.

Thermal Melting Studies. Thermal melting experiments were conducted with a Cary 219 spectrophotometer interfaced to an Apple IIe microcomputer. The temperature of the Cary was controlled by a Haake PG20 temperature programmer connected to a Haake A81 refrigerated bath which was set to raise the temperature at 0.5 °C/min. A thermistor fixed into a reference cuvette was used to monitor the temperature. The polymers were added to 1 mL of buffer in 1-cm path length reduced volume quartz cells, and the concentration was determined by measuring the absorbance at 260 nm. Experiments were generally conducted at a 5×10^{-5} M concentration of DNA base pairs and at saturating concentrations of added compound (0.6 mol of compound/mol of base pair).

Kinetics. Kinetics measurements were conducted with a Hi-Tech SF-51 stopped-flow spectrometer interfaced to an HP 330 computer as previously described (Tanious et al., 1991; Wilson et al., 1990b). The SF-51 is equipped with a micromixing chamber and a microcell that allow use of less than 50 μL of sample solution in each mixing event. Single-wavelength kinetic records of absorbance or fluorescence versus time were collected.

Molecular Modeling. All modeling studies were conducted with the Tripos SYBYL 5.4 modeling package and a Silicon Graphics IRIS 4D/25 computer networked to a Silicon Graphics 4D/380S. The force field and potential energy equation used for calculations have been described previously (Veal & Wilson, 1991). The force field is a modification of that described by Kollman and co-workers (1986) for modeling nucleic acids. A 15-Å cutoff was used for nonbonded interactions, and full relaxation of atomic bond stretch, angle bend, and torsional parameters was allowed. A distance-dependent dielectric constant, $\epsilon = 4r_{ij}$, was used in calculating the electrostatic energy, and phosphates charges were reduced to their apparent solution value of −0.2. A conjugate gradient method was used for minimizations, and the convergence criteria for a minimized structure was a change in the rms gradient of less than 0.05 kcal/(mol·Å^2).

The starting conformations for nucleic acids were generated from general fiber diffraction data (Arnott et al., 1972). The structures were then modified to have standard terminal 5′- and 3′-OH groups and were energy minimized. The inter-

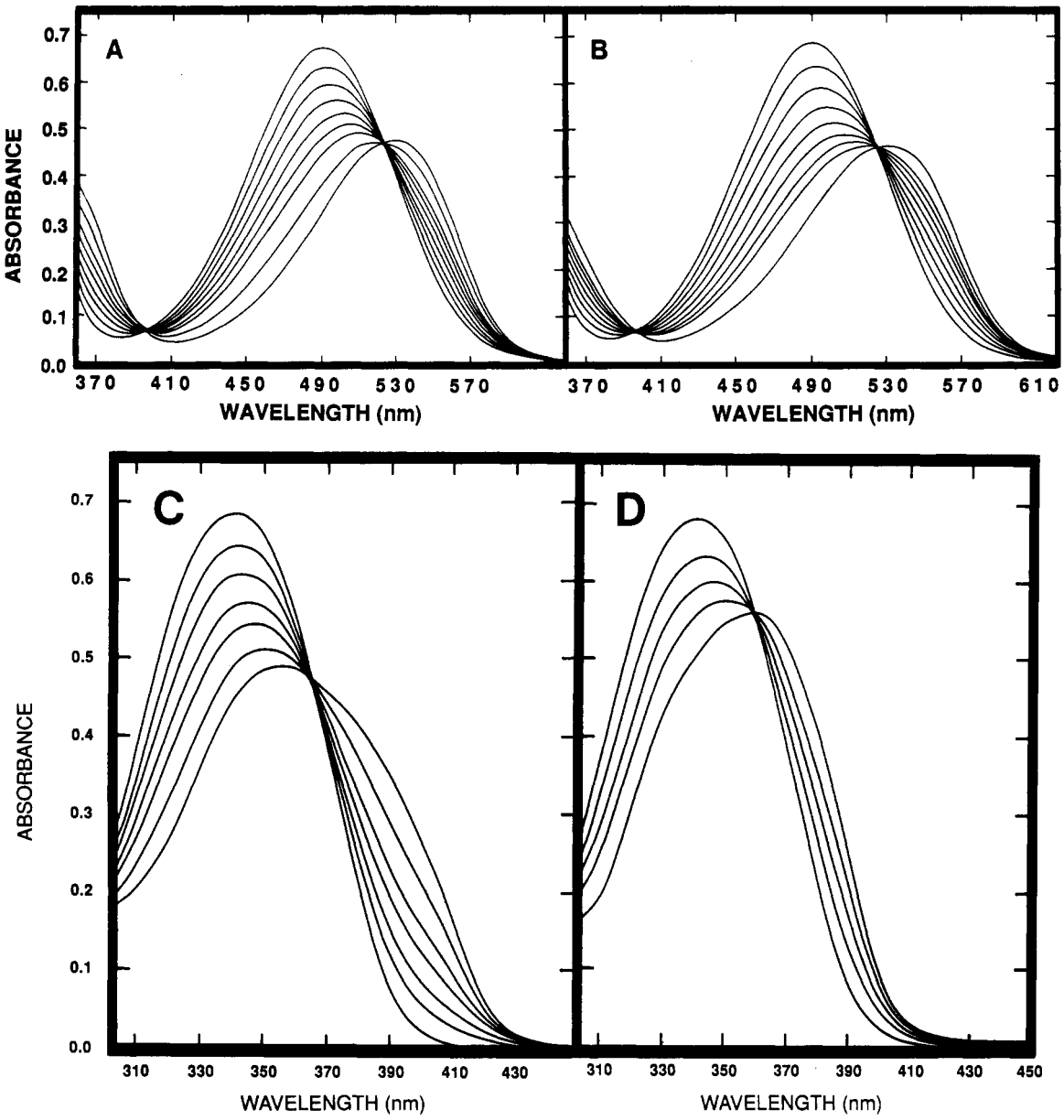

FIGURE 3: Spectral shifts of propidium (1.1×10^{-4} M) on titration with (A) polyA·polyU and (B) polydA·polydT. In (A), the polymer base pair molarity is (top to bottom curves at 493 nm): 0, 0.37, 0.74, 1.11, 1.48, 1.85, 2.22, 2.94, and 4.02×10^{-4}. In (B), the polymer base pair molarity is (top to bottom curves at 493 nm): 0, 0.37, 0.74, 1.11, 1.47, 1.82, 2.18, 2.52, and 3.89×10^{-4}. Spectral shifts of DAPI (2.5×10^{-5} M) on titration with polyA·polyU (C) and (D) polydA·polydT. In (C), the polymer base pair molarity is (top to bottom curves as 340 nm): 0, 1.1, 2.3, 4.2, 6.1, 9.8, and 15.4×10^{-5}. In (D), the polymer base pair molarity is (top to bottom curves at 340 nm): 0, 2.3, 4.2, 6.0, and 9.7×10^{-5}. All titrations were conducted in 1-cm cuvettes in MES buffer with 0.1 M NaCl at 25 °C in a Cary 2200 spectrophotometer.

calation sites were generated by applying a large number of distance and torsional constraints on the basis of crystallographic data (Neidle, 1989), as described previously (Veal & Wilson, 1991), to the minimized nucleic acid structure and reminimizing. DAPI was modeled with partial charges calculated from MNDO (QCPE-AMPAC) and was manually docked with intercalation and minor-groove sites in a number of initial conformations prior to complex minimization. A detailed analysis of the modeling of a range of unfused aromatic compounds with nucleic acids will be presented elsewhere (J. M. Veal, R. L. Jones, and W. D. Wilson, manuscript in preparation).

RESULTS

Viscometric Titrations. Results for viscometric titrations of polyA·polyU with propidium, DAPI, and distamycin at 30 °C in MES buffer are shown in Figure 2S (supplementary material). Both DAPI and propidium increase the reduced specific viscosity of polyA·polyU in a manner characteristic of intercalation binding (Waring, 1981; Wilson & Jones, 1981). Propidium increases the reduced specific viscosity ratio of polyA·polyU (maximum of 2.4) slightly more than DAPI. Other dicationic intercalators such as the acridine, quinacrine, cause increases (maxima 1.8–2.0) quite similar to those observed with DAPI. The titrations level off in the molar ratio range of 0.3–0.4 (compound/polymer base pair) for DAPI and propidium, but the reduced specific viscosity of polyA·polyU with DAPI decreases at molar ratios greater than 0.4, probably due to secondary binding modes and/or aggregation at the high ratio of compound/polymer base pairs.

Spectrophotometric Titrations: Propidium. Titrations of propidium in the UV–visible region with the nonalternating polymers polyA·polyU and polydA·polydT are shown in panels A and B, respectively, of Figure 3. The spectrum for free propidium in solution has an absorbance maximum at 493 nm, and following addition of either polymer, there is significant

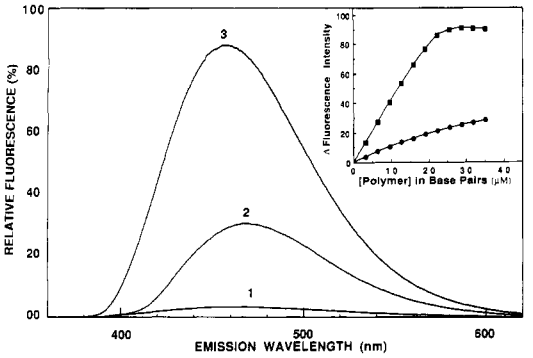

FIGURE 4: Fluorescence emission spectra of DAPI (1) at 25 °C in MES buffer with 0.1 M NaCl and of DAPI complexes with polyA·polyU (2) and polydA·polydT (3). The excitation wavelength was at 350 nm, and the molar ratio was 0.17 DAPI/base pairs for both complexes. The inset shows titrations of 6×10^{-6} M DAPI in MES buffer with 0.1 M NaCl at 25 °C with polyA·polyU (●) and polydA·polydT (■).

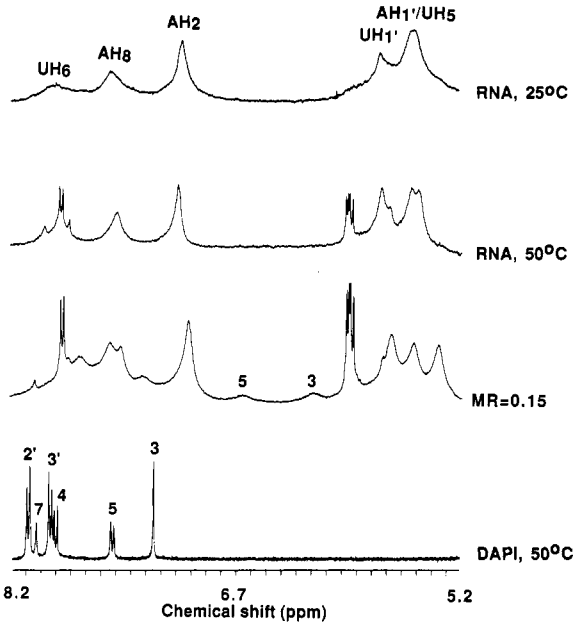

FIGURE 5: ^{1}H NMR spectra of the aromatic and suger H1′ proton region of DAPI complexes with sonicated polyA·polyU at 50 °C in D_2O. Spectra for polyA·polyU are shown at 25 °C and 50 °C at the top of the figure. The molar ratio of DAPI to base pairs in the complex was 0.15. Spectra were collected on a Varian VXR 400-MHz spectrometer in MES buffer with 0.1 M NaCl.

hypochromicity and a red shift of the absorbance maximum. The propidium extinction coefficient at 494 nm is 6060 M^{-1} cm^{-1} in the free state and decreases to 2290 M^{-1} cm^{-1} and 2070 M^{-1} cm^{-1} when bound to polyA·polyU and polydA·polydT, respectively. For titrations with either polymer, the absorbance maximum for propidium in the bound state is shifted to 532 nm, and isosbestic points are obtained at 395 and 524 nm. In summary, the absorbance maximum, isosbestic points, and total hypochromicity are very similar for propidium complexed with polyA·polyU and polydA·polydT.

Spectrophotometric Titrations: DAPI. Titrations of DAPI with polyA·polyU and polydA·polydT are shown in panels C and D, respectively, of Figure 3 in the 310–450-nm spectral region. The spectrum for free DAPI in solution has an absorbance maximum at 340 nm (the extinction coefficient is 27 000 M^{-1} cm^{-1}), and as either polymer is added, hypochromicity changes and a red shift in the spectrum are observed as with propidium. Unlike propidium, however, there are significant differences in both the degree of hypochromicity and the nature of the spectrum of the bound species when DAPI interacts with the nonalternating DNA and RNA polymers. For DAPI bound to polydA·polydT, the extinction coefficient is 19 500 M^{-1} cm^{-1} at 340 nm, but for DAPI bound to polyA·polyU, the extinction coefficient at 340 nm is much lower, 14 500 M^{-1} cm^{-1}. Additionally, when DAPI is fully complexed with polyA·polyU, its absorbance maximum is shifted to 360 nm, and an isosbestic point occurs at 365 nm. When DAPI is fully complexed with polydA·polydT, the degree of red shift in the spectrum is reduced, with the DAPI absorbance maximum at 358 nm and an isosbestic point occurring at 360 nm. For polyA·polyU at salt concentrations below 0.05 M, isosbestic behavior was lost, presumably due to nonspecific, electrostatic interaction of DAPI with the RNA phosphate backbone as observed by Manzini et al. (1985).

Fluorescence Titrations: DAPI. Fluorescence spectra of free DAPI and DAPI complexed with polyA·polyU and polydA·polydT are shown in Figure 4. Free DAPI has a fluorescence maximum at 461 nm. Addition of polydA·polydT causes a large increase in the fluorescence intensity and a shift of the fluorescence maximum to a lower wavelength (456 nm). Addition of polyA·polyU causes a significantly smaller increase in the fluorescence intensity and a red shift of the peak maximum to longer wavelength (468 nm). The differences in fluorescence enhancement in titrations of DAPI with polyA·polyU and polydA·polydT are shown in the inset Figure 4. The fluorescence results, as with the absorption spectroscopy studies, again indicate that the modes of interaction of DAPI with polyA·polyU and polydA·polydT are different.

Proton NMR Titrations: DAPI. Proton NMR spectra in the aromatic and sugar H1′ region of polyA·polyU are shown at 25 °C and 50 °C in Figure 5. The proton chemical shift at 25 °C are in good agreement with published results for duplex polyA·polyU (Leroy et al., 1985; Rycyna, 1986). At 50 °C some sharp lines, characteristic of the single-stranded polymer, are seen as unfolding and denaturation begin (Rycyna, 1986). Addition of the RNA polymer to DAPI at 25 °C results in broad lines in the NMR spectra and some precipitation of the sample. At 50 °C the lines are sharper and the complex is in fast exchange on the NMR time scale, although at high ratios of DAPI to polymer base pairs precipitation still occurs. At ratios of 0.3 (DAPI to base pair) and below, a soluble complex is obtained at 50 °C, provided the DAPI concentration is kept below 1 mM. Spectra of free DAPI and of DAPI complexed with RNA at molar ratio of 0.15 and 50 °C are shown in Figure 5. The 3 and 5 protons of the indole ring of DAPI are resolved in the complex and are labeled in Figure 5. It is clear from comparison of free and complexed spectra that all protons of DAPI are shifted significantly upfield (>0.5 ppm) on complex formation. No significant broadening or chemical shift changes were observed for the single-stranded RNA on addition of DAPI.

Thermal Melting Studies. A qualitative comparison of the relative binding strengths of the compounds of Figure 1 with polydA·polydT and polyA·polyU sequences is obtained by comparison of the relative increases they induce in the T_m of these polymers (Cantor & Schimmel, 1980; Crothers, 1971). DAPI and distamycin give exceptionally large T_m increases with polydA·polydT, but propidium gives larger increases with polyA·polyU (Table I). Distamycin causes less than a 1 °C increase in T_m of the AU sequence, and it presumably interacts with RNA only through a very weak electrostatic, external mode.

Propidium Dissociation Kinetics: Effects of Salt Concentration. The fluorescence changes observed on binding of propidium to polydA·polydT and polyA·polyU polymers were

Table I: Thermal Melting Studies[a]

compound	polyA·polyU ΔT_m (°C)	polydA·polydT ΔT_m (°C)
propidium	24.6	16.7
DAPI	4.0	27.0
quinacrine	8.1	18.6
distamycin A	0.5	25.5

[a] Experiments were conducted in MES buffer with 0.1 M added NaCl. Polymer T_ms are 67.0 °C for polydA·polydT and 57.0 °C for polyA·polyU.

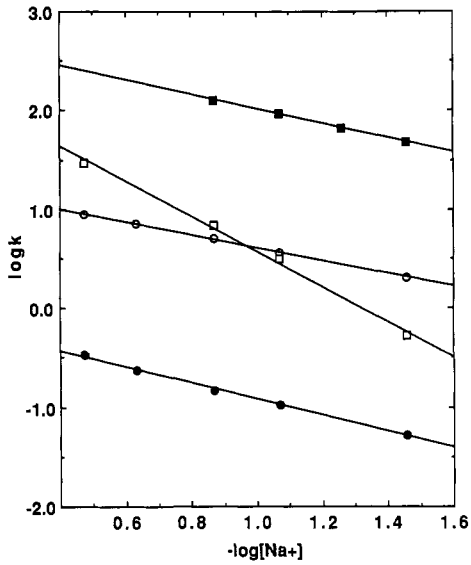

FIGURE 7: Plots of log k_{app} vs −log [Na^+] for dissociation of propidium from polydA·polydT (○); polyA·polyU (●); and DAPI from polydA·polydT (□); polyA·polyU (■). Experiments were conducted in MES buffer at different ionic strengths in the manner described in Figures 6S and 8.

used to monitor the kinetics of SDS-induced dissociation (Figure 6S, supplementary material). Dissociation of propidium from polyA·polyU is much slower than from polydA·polydT in agreement with the stronger binding of propidium to polyA·polyU. Single-exponential curves give satisfactory fits to the data and two exponential fits do not significantly improve the residuals or rms deviations (Figure 6S). Dissociation kinetics experiments were conducted at constant temperature as a function of salt concentration, and plots of log k as a function of −log [Na^+] are shown in Figure 7. The slopes for the dissociation of propidium from the complexes are 0.8 for polyA·polyU and 0.7 for polydA·polydT.

DAPI Dissociation Kinetics: Effects of Salt Concentration. Both fluorescence and absorption spectral changes observed on binding of DAPI to polydA·polydT and polyA·polyU polymers were used to monitor the kinetics of binding as with propidium. Both methods gave the same results within experimental error, and a plot of absorption spectral changes as a function of time is shown in Figure 8. Consistent with the stronger binding of DAPI to the DNA polymer, DAPI dissociates much more slowly from polydA·polydT than from polyA·polyU. Unlike the propidium data, single-exponential fits give unsatisfactory residuals and significantly higher rms deviations with DAPI complexes with both polymers than two-exponential fits (Figure 8). Three exponential fits do not significantly improve the residuals or rms deviations. With both DNA–DAPI and RNA–DAPI complexes, the amplitude for the fast phase of the dissociation reaction accounts for ~30% of the total amplitude under all conditions used, and the relative amplitude of the fast phase increases slightly with increasing salt concentration.

Table II: Salt Dependence of DAPI Dissociation Rate Constants[a]

[Na^+]	k_1 (s^{-1})	% A_1	k_2 (s^{-1})	% A_2	τ(s)
		polyA·polyU			
0.035	60.70	42.9	25.00	57.1	0.0248
0.055	99.90	39.4	47.50	60.6	0.0147
0.085	130.0	24.0	80.40	76.0	0.0108
		polydA·polydT			
0.035	1.08	32.0	0.263	68.0	1.907
0.085	6.93	32.9	1.89	67.1	0.282
0.135	14.3	28.6	3.95	71.4	0.145
0.335	69.4	23.7	17.0	76.34	0.034

[a] All experiments were conducted in MES buffer at 20 °C for polydA·polydT and at 15 °C for polyA·polyU.

Table III: Equilibrium Constants Calculated from Kinetic Results[a]

complex	$k_a \times 10^{-6}$ (M^{-1} s^{-1})	k_d (s^{-1})	$K \times 10^{-4}$ [b]
DAPI–polyA·polyU	6.4	129	5.0
DAPI–polydA·polydT	63.3	8.5	740
DAPI–poly[d(G-C)]$_2$[c]		220	12

[a] Experiments were conducted in MES buffer with 0.1 M added NaCl at 15 °C. k_a and k_d values are from the slopes and intercepts of Figure 10. [b] Equilibrium constant calculated from the value of k_a/k_d [c] Data from Wilson et al. (1990b); the equilibrium constant is the directly determined experimental value.

For the purposes of comparison, the dissociation lifetime (τ) and apparent rate constant ($k_{app} = 1/\tau$) were calculated from the computer-derived, best-fit values for rate constants and amplitudes:

$$\tau = 1/(A_1k_1 + A_2k_2) \quad (1)$$

where A and k values refer to the amplitudes and rate constants for the two-exponential fits to the dissociation results (Table II). As with propidium, dissociation rate constants were measured as a function of salt concentration at constant temperature, and the results are collected in Table II. Plots of log k_{app} as a function of −log [Na^+] are shown in Figure 7, and quite different results are obtained with the DNA and RNA polymers. For the SDS-driven dissociation of DAPI from polyA·polyU, a slope of 0.7, similar to the propidium results, is obtained, but with polydA·polydT a slope of 1.8 ± 0.1, similar to the slope for the DAPI–poly[d(A-T)]$_2$ complex (Wilson et al., 1990b), is obtained. It is clear from these results that binding of DAPI to dAT and rAU sites follow quite different mechanisms.

DAPI Association Kinetics. As an additional probe for the binding modes of DAPI to AT sequences in DNA and AU sequences in RNA, association kinetics for the interaction of DAPI with these nucleic acids have been monitored. Experimental traces of fluorescence versus time are plotted under similar conditions in Figure 9 for binding of DAPI to RNA and DNA polymers. Experiments such as those shown in Figure 9 were repeated at range of polymer concentrations under different salt conditions to determine the second-order association rate constants according to the equation

$$k_{obs} = k_a[\text{polymer}] + k_d \quad (2)$$

where k_{obs} is the experimentally observed pseudo-first-order rate constant, [polymer] is the nucleic acid concentration in base pairs, k_a is the association rate constant, and k_d is the dissociation rate constant. The association rate constant for DAPI with the AT polymer is clearly much larger than with the AU polymer (shown in Table III at 0.1 M NaCl). The ratio of association-to-dissociation rate constants gives an apparent equilibrium constant (Table III). As can be seen from these results, DAPI binds strongly to both polymers but binds >100 times more strongly to polydA·polydT. Results for DAPI interaction with poly[d(G-C)]$_2$ (Wilson et al.,

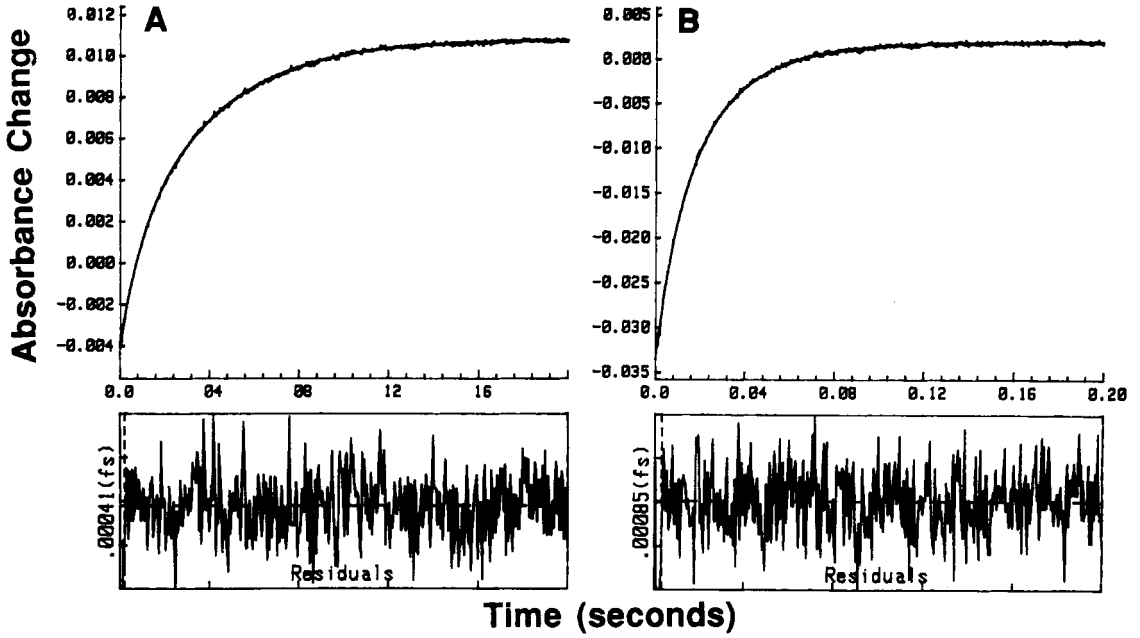

FIGURE 8: Stopped-flow kinetics traces for the SDS-driven dissociation of DAPI (A) from polydA·polydT and (B) from polyA·polyU. The experiments were conducted at 20 °C in MES buffer with no added salt at a ratio of 1:10 DAPI to polymer base pairs. The concentration of DAPI after mixing was 1.25×10^{-5} M. The smooth lines in panel A and panel B are the two-exponential fits to the data. Residual plots for the fits are shown under each experimental plot.

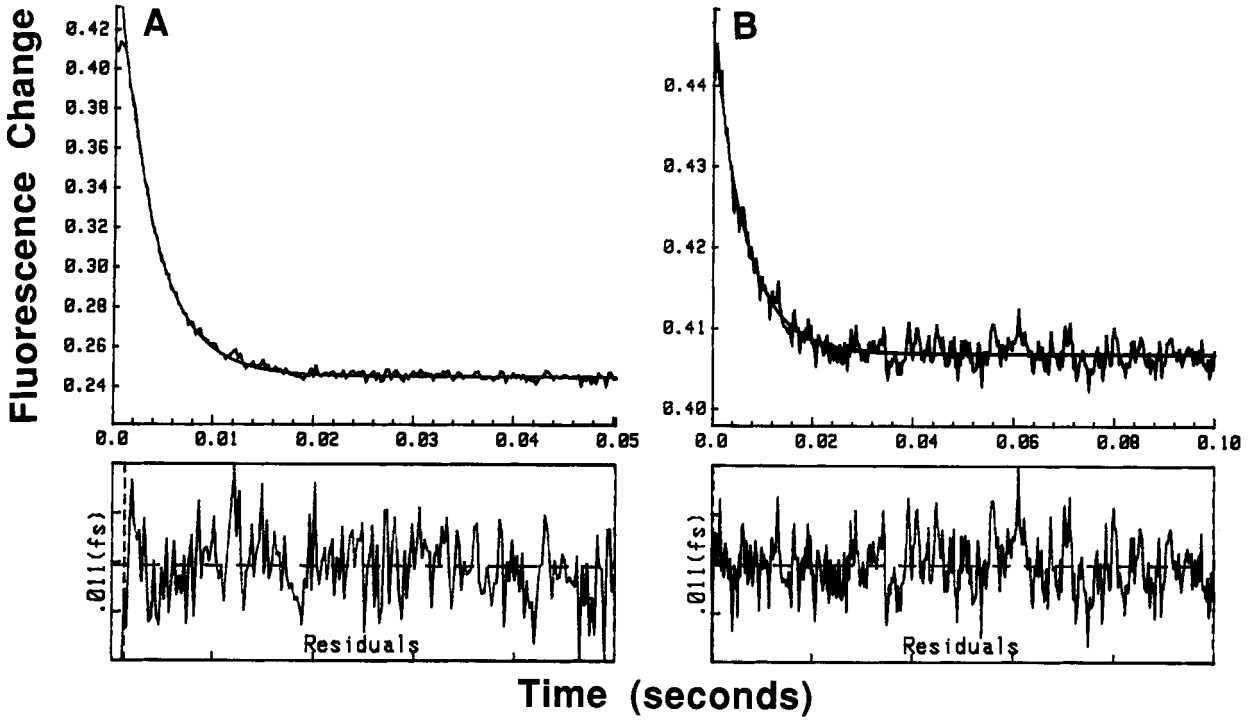

FIGURE 9: Stopped-flow kinetics association reactions of DAPI (A) with polydA·polydT and (B) with polyA·polyU. The experiments were conducted at 15 °C in MES buffer with 0.2 M Na^+ at a ratio of 1:10 DAPI to polymer base pairs. The concentration of DAPI after mixing was 4×10^{-7}M. The smooth lines in panel A and panel B are the single-exponential fits to the data. Residual plots for the fits are shown under each experimental plot.

1990b) are included in Table III for comparison. The k_a value for DAPI association with AT base pairs has a very low salt dependence (log k_a vs −log [Na^+] slope of −0.3) and is approximately $\sim 10^8$ M^{-1} s^{-1} across the experimental salt concentration range (Lohman et al., 1978; Lohman, 1985; Wilson et al., 1985a, 1989b, 1990a,b). The association rate constant for the binding of DAPI to AU sequences in RNA is considerably more dependent on salt concentration (log k_a vs −log [Na^+] slope of −1.5).

Molecular Modeling. An intercalation site was created between the central base pairs of the octamer model $A_8 \cdot U_8$ as previously described (Veal & Wilson, 1991) by using crystallographic coordinates (Neidle, 1989) as a guide for the intercalation site and A-form fiber diffraction coordinates for the other bases (Arnott et al., 1972). DAPI was visually docked into the intercalation site with a real time display of selected distances. Three different complex geometries, with the amidines in the minor groove and in the major groove and with one amidine in each groove (threading), were tested. Complex energies were also monitored to obtain a low-energy initial structure without geometry optimization. The complexes were then energy minimized by using a force field

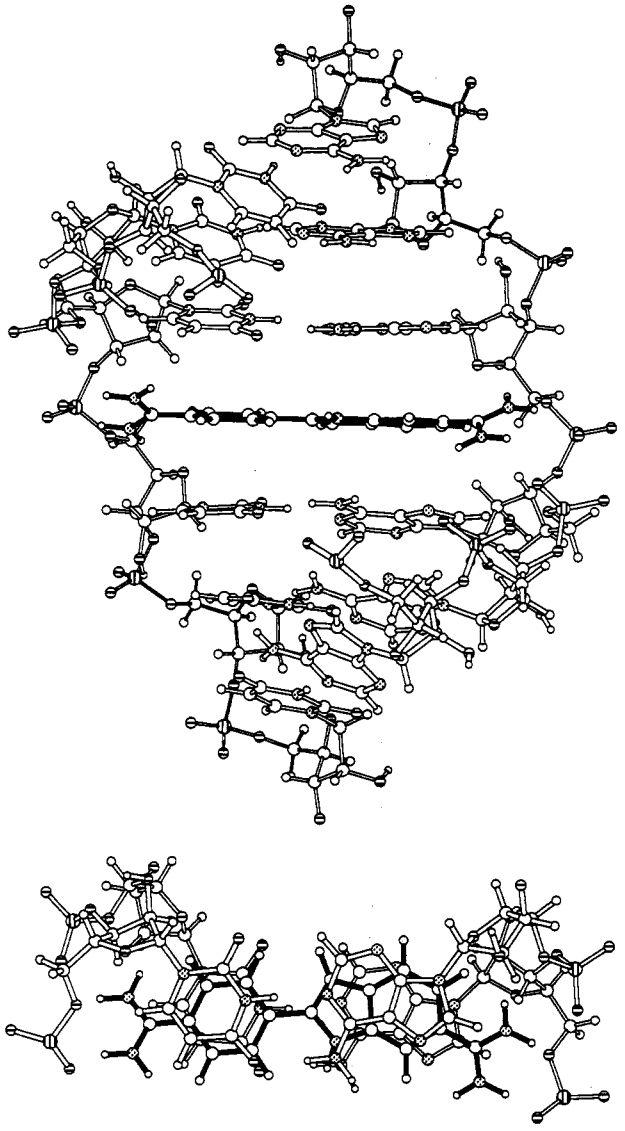

FIGURE 10: Views of the complex of DAPI with r(A_8·U_8). (Top) The view shown is into the major groove of the internal six base pairs of r(A_8·U_8) with DAPI intercalated in the center. The indole ring is on the right, stacked between adenosines, and the phenyl ring is on the left between uracils. Base pair propeller twist can be easily seen in this view, and the DAPI indole–phenyl bond is twisted by approximately 8° to match the base pair propeller twist. The amidine groups are rotated 31° with respect to the indole and 32° with respect to the phenyl rings to which they are attached and interact with the phosphate groups that line the walls of the major groove in the RNA complex. (Bottom) A top view of DAPI stacked with the central two base pairs of the DAPI–r(A_8·U_8) complex is shown. The indole and adenosines are on the right with the phenyl and uracils on the left. The minor groove is at the top and the major groove is at the bottom of this view. Carbon and hydrogen are white, nitrogen atoms are stippled, phosphorus has horizontal lines, and oxygen has vertical lines. DAPI bonds are black for visualization of the bound molecule.

developed for modeling cationic drug–nucleic acids interactions (Veal & Wilson, 1991). The intercalation complex with the amidine groups in the minor groove has the highest energy, and favorable van der Waals contacts, electrostatic interactions, and hydrogen bonding are significantly reduced relative to the other complexes. The complex with amidine groups in the major groove has the lowest energy of the three binding modes. The lowest energy major-groove complex has the indole ring of DAPI stacked between adenosines on the purine strand and the phenyl ring system between uracils on the pyrimidine strand of A_8·U_8 (Figure 10). As can be seen, DAPI bound in this orientation forms excellent van der Waals contacts with the bases and the phenyl and indole rings of DAPI are able to rotate slightly to match the propeller twist of the base pairs at the intercalation site. Additionally, the DAPI amidine groups have close contacts with phosphate groups in the RNA major groove leading to both favorable hydrogen bonding and electrostatic interactions.

An A-form RNA helix of A_8·U_8 without the intercalation site was also generated from fiber diffraction coordinates (Arnott et al., 1972) and energy minimized. DAPI was then docked into the minor groove of the helix. On energy minimization, DAPI forms close contacts with one strand of the shallow A-form minor groove and contacts with the edges of the central four AU base pairs at the floor of the groove. The total number of favorable contacts, however, is much reduced relative to those observed in the DAPI minor-groove complex with dA·dT in DNA (Larsen et al., 1989). In the DNA complex, the deep narrow minor groove permits numerous contacts with the sugar phosphate backbone of both strands where, as noted, in the RNA complex with wide, shallow groove geometry only permits a small number of primary contacts with one strand. The van der Waals, electrostatic, and hydrogen-bonding interaction energy sum in the RNA intercalation complex is calculated to be −64 kcal/mol, and it is only −36 kcal/mol for the DAPI complex in the A_8·U_8 minor groove. With DNA AT sites, the minor groove complex has a lower interaction energy than the intercalation complex.

Discussion

While the intercalation and minor-groove-binding modes of organic cations with DNA have been well characterized (Waring, 1981; Wilson, 1990), substantially less information is available on similar complexes with RNA. Two compounds that have been studied, the monocationic and dicationic phenanthridinium derivatives, ethidium and propidium, form similar intercalation complexes with DNA and RNA (Davidson et al., 1977; Bresloff & Crothers, 1981; Waring, 1981; Nelson & Tinoco, 1984; Wilson et al., 1985a,b, 1986; Babayn et al., 1987). Ethidium intercalation complexes with both DNA and RNA dinucleotides have been crystallized, and the overall geometries of the two complexes are quite similar (Jain & Sobell, 1984a,b; Neidle, 1989). NMR studies indicate that the ethidium and propidium complexes have similar intercalation conformations in solution (Patel, 1979; Krugh & Nuss, 1979; Davidson et al., 1977). DAPI binding to both RNA and DNA has also been previously studied, and the minor groove binding mode of DAPI in AT regions of DNA has been extensively characterized (Kapuscinski & Szer, 1979; Pullman & Pullman, 1981; Manzini et al., 1985, 1983; Zimmer & Wahnert, 1986; Dervan, 1986; Kubista et al., 1987; Portugal & Waring, 1988; Larsen et al., 1989; Wilson et al., 1990). A crystal structure of such a DAPI–DNA complex provides a detailed model for DAPI minor groove binding (Larsen et al., 1989).

Although it has been proposed that DAPI binds in the minor groove in AU regions of RNA (Manzini et al., 1985) as with AT regions of DNA, no crystallographic or NMR-based models for such an RNA complex are available. The minor groove of RNA is in fact very different from the minor groove of DNA, and in particular is more shallow, wide, and electrostatically positive (Pullman & Pullman, 1981; Saenger, 1984; Blackburn & Gait, 1990; Veal & Wilson, 1991). All of these characteristics create a significantly less favorable environment for a minor-groove-binding mode of interaction. Because of our desire to design RNA interactive drugs, we have investigated DAPI binding to polyA·polyU with a number of experimental techniques to determine the mode of binding.

Results from viscosity, spectroscopy, and kinetics experiments indicate that DAPI intercalates into polyA·polyU sequences. Moreover, since models exist for propidium intercalating into DNA and RNA, and for DAPI binding in the minor groove of DNA in AT sequences, we have used comparisons of experimental results for DAPI and propidium binding to both RNA and DNA to assist in characterization of the DAPI–RNA binding mode.

Viscosity. Large increases in the reduced specific viscosity of nucleic acid solutions upon addition of an organic cation provide a fundamental test for intercalation (Waring, 1981; Wilson & Jones, 1981). Consistent with intercalation, titration of a polyA·polyU solution with DAPI causes significant increases in the reduced specific viscosity (Figure 2S), and the magnitude of the change is similar to that seen for intercalators. Conversely, distamycin binds very weakly and causes slight decreases in RNA solution viscosity that are characteristic of simple electrostatic interactions.

Spectroscopy. Visible spectroscopy studies of DAPI and propidium complexes with polyA·polyU and polydA·polydT also provide results which are supportive of DAPI intercalation into polyA·polyU. The propidium absorption spectrum shifts to longer wavelengths and displays large hypochromicity on binding to both RNA and DNA (Figure 3). The absorption spectral changes are similar for the two polymers in agreement with an intercalation binding mode for propidium with both RNA and DNA. With DAPI, however, the spectral changes on binding to the RNA and DNA polymers (Figure 3) are quite distinct. Larger shifts to longer wavelengths and significantly greater hypochromicity are seen when DAPI binds to the RNA than to the DNA polymer. These more pronounced changes occur even though the binding affinity for DAPI with polyA·polyU is significantly less than for DAPI with polydA·polydT. Given that DAPI binds in the minor groove in AT sequences, the large spectral shifts of DAPI bound to polyA·polyU do not seem consistent with binding to the wide and shallow RNA minor groove. The spectral changes can be readily explained, however, by an intercalation model in which the pronounced hypochromicity and larger red shifts are attributed to stacking with adjacent base pairs at the intercalation site.

Fluorescence spectroscopy also supports distinct binding modes for DAPI with the RNA and DNA polymers. Whereas the fluorescence maximum for DAPI shifts to shorter wavelengths upon complexation with polydA·polydT, it shifts to longer wavelengths upon complexation with polyA·polyU (Figure 4). Moreover, the fluorescence enhancement is much smaller for DAPI binding to the RNA than to the DNA polymer.

Large upfield chemical shifts in ligand aromatic resonances are seen in NMR spectra upon intercalative binding to DNA and RNA due to base pair ring current shielding effects (Patel, 1979; Chandrasekaran et al., 1986; Wilson et al., 1992). Conversely, minor groove binding leads to chemical shift changes of significantly smaller magnitude which can be either upfield or downfield. The large upfield NMR chemical shift changes in DAPI resonances upon complexation with polyA·polyU (Figure 5) are only consistent with an intercalation binding mode with the RNA polymer. Conversely, under similar conditions, DAPI protons show small chemical shift changes upon titration with polyd(A-T)$_2$, and for resonances 3 and 5, they are downfield (Wilson et al., 1990a,b) whereas they are upfield with RNA. The chemical shift changes for DAPI with polyA·polyU are similar to those observed for the DAPI intercalation with poly[d(G-C)]$_2$; the H3 proton of DAPI, for example, shifts upfield approximately 0.9 ppm (Wilson et al., 1989b, 1990a,b) with both polymers.

Kinetics. The mechanisms of intercalation and groove-binding modes are distinctly different, and kinetics experiments are, thus, quite useful in establishing complex binding modes (Lohman et al., 1978; Lohman, 1985; Wilson et al., 1985a, 1989b, 1990a,b). For all compounds, dissociation rate constants increase and dissociation rate constants decrease as the salt concentration is increased. Slopes of log k vs $-\log [Na^+]$ plots for both association and dissociation are particularly useful in distinguishing the binding mode. For dications, slopes of such plots for dissociation reactions are predicted to be 0.6–0.8 for intercalation and 1.6–1.8 for minor groove complexes. The slopes for dication association reactions are predicted to be ~ -1.4 for intercalation and ~ -0.24 for groove binding (Wilson et al., 1985a, 1990b). The dissociation of propidium from its RNA complex is ~40 times slower than from its DNA complex, but the log k vs $-\log [Na^+]$ slopes are very similar for both the RNA and DNA complexes and are consistent with an intercalation binding mode to both polymers.

DAPI dissociates ~100 times more slowly from the DNA than the RNA complex, but unlike the propidium complexes, the log k vs $-\log [Na^+]$ slopes are quite different (Figure 7). The dissociation slope for the DAPI–DNA complex is 1.8 in agreement with the expected groove-binding mode in AT sequences. The slope for the RNA complex, however, is 0.7, similar to the propidium complex value, and consistent with an intercalation binding mode for DAPI with RNA. The association kinetics log k_a vs $-\log [Na^+]$ slopes are even more strikingly different for the DAPI complexes with DNA and RNA. The slope for the DNA complex is very low (−0.3) in agreement with minor-groove association, while the RNA complex slope is −1.5, again consistent with an intercalation binding mode.

Kinetic and equilibrium results are compared in Table III for DAPI binding to polyA·polyU, polydA·polydT, and poly-[d(G-C)]$_2$. As can be seen, the DAPI kinetic and equilibrium results with AU sites in RNA are more similar to results for intercalation at GC sites in DNA than for groove binding at AT sites in DNA. The DNA minor groove at consecutive AT base pairs clearly presents a very favorable binding site. In all other regions of DNA and in RNA, however, DAPI binds by intercalation with a binding constant in the range typically seen for intercalators such as ethidium and quinacrine (Wilson et al., 1989b, 1990a,b).

The association rate constant for the DAPI–DNA complex (minor groove binding) is near the diffusion-controlled limit while the rate constant for the DAPI–RNA complex (intercalation) is significantly lower. Macgregor and Clegg (1987) have shown that intercalation of ethidium has a slow step that depends on the DNA conformational transition required to create an intercalation site. Groove binding of DAPI, at least into AT polymers, does not appear to require a significant DNA conformational change and thus, approaches the diffusion limit.

Modeling. In an effort to better understand RNA interactions, in general, and the RNA–DAPI complex, in particular, an RNA intercalation site was generated in the nonalternating sequence A_8·U_8. Both DAPI and propidium were docked into this site and into a similar site in the DNA sequence dA_8·dT_8 for comparison. DAPI was also docked into the minor groove of both sequences without the intercalation site. Propidium fits well into both the RNA and DNA intercalation sites with the phenyl and alkyl substituents in the minor groove as previously described for ethidium (Veal &

Wilson, 1991). DAPI forms a strong complex in the minor groove of $dA_8 \cdot dT_8$ that has better energetics than the intercalation complex. With RNA, however, the minor groove geometry is very different than in DNA, and many of the favorable interactions that occur in the DNA minor-groove complex are not possible with RNA (Figure 10). DAPI fits quite well into the RNA intercalation site, however, and better interaction energetics are obtained for DAPI intercalation than for groove binding with RNA.

We have previously shown that DAPI forms a very strong intercalation complex in GC sequences in DNA (Wilson et al., 1989b, 1990a,b), where the minor groove does not present a favorable binding site due to steric restrictions by the G NH_2 group, and such a complex also accounts for the experimental results for the DAPI–RNA complex. The low energy complex in the DNA GC site for DAPI has both amidine groups projecting into the major groove. This is also the optimum orientation for the DAPI–RNA intercalation complex, and as can be seen from Figure 10, many favorable interactions between the RNA intercalation site and the DAPI molecule are possible in a complex with this orientation.

It should be noted that direct comparisons between the relative energetics of complex formation in the minor groove and in an intercalation site are difficult. Creation of an intercalation site involves the energy cost of unstacking the bases along with secondary effects such as changes in phosphate–phosphate distance and resulting electrostatic interactions. X-ray crystallographic analysis of DNA oligomers and their complexes with minor-groove-binding ligands such as DAPI, however, have indicated that the DNA conformation undergoes only small changes between the free oligomer and the complexed form (Larsen et al., 1989). The X-ray results have also indicated that the grooves of nucleic acids are extensively hydrated and much of the minor-groove water of hydration is displaced from the binding site by minor-groove ligands. Disrupting this minor-groove hydration matrix is clearly a positive energy step in minor-groove interactions, but we do not have good models for estimating the energetics involved. We are working on such estimations but, at present, have simply focused on the energetics of interaction between the ligand and the binding site for comparison purposes. Within this limitation, however, the modeling results completely support the experimental findings. In DNA AT sites, the energetics are more favorable for a minor groove than for an intercalation complex. In RNA AU sites, the energetics are reversed and intercalation is more favorable than minor-groove binding.

Conclusions. The results of this paper allow several generalizations concerning RNA binding modes and how they are related to binding modes in DNA. First, as has been pointed out previously (Neidle, 1989; Veal & Wilson, 1991), generation of an intercalation site in the A-form of RNA is quite straightforward, and the geometry of the site is similar to DNA intercalation sites. Depending on the structure of the intercalator and local variations in sequence and conformation, binding may be stronger to either RNA or DNA.

Second, the favorable characteristics of the minor groove in AT sequences for binding of molecules such as netropsin, distamycin, and DAPI have been defined in detail (Pullman & Pullman, 1981; Kopka et al., 1985a,b,c; Zimmer & Wahnert, 1986). The 2-NH_2 group of G sterically inhibits such binding, and molecules that bind in the minor groove in AT sequences either bind weakly (e.g., netropsin and distamycin) or they bind more strongly but by an intercalation mode (DAPI and structurally related unfused aromatic compounds) in GC sequences. Molecules such as distamycin do not form intercalation complexes and, thus, bind weakly, probably through simple external electrostatic interactions, to AU sequences in RNA even though no G NH_2 group is present. DAPI binds to RNA much more strongly than distamycin, but it does so not through a groove complex but through an intercalation complex that is similar to the DAPI complex with GC sequences in DNA.

Finally, from the standpoint of the design of potential drugs that target RNA, we have excellent paradigms for the design of RNA intercalators, but there are, at present, *no paradigms for the design of RNA groove-binding molecules.* The deep and narrow major groove of RNA may be a better receptor of aromatic cations than the wide shallow minor groove. We are perusing the design of RNA selective major-groove specific molecules through computer-based molecular modeling methods.

Acknowledgments

We thank the reviewers for helpful comments, particularly concerning the kinetics experiments.

Supplementary Material Available

Two figures and captions showing the viscometric titrations of polyA·polyU with propidium, DAPI, and distamycin (Figure 2S) and the stopped-flow kinetic traces for the SDS-driven dissociation of propidium from polydA·dT and from polyA·polyU (3 pages). Ordering information is given on any current masthead page.

References

Arnott, S., Hukins, D. W. L., & Dover, S. D. (1972) *Biochem. Biophys. Res. Commun. 48*, 1392–1399.

Babayan, Y., Manzini, G., Xodo, L., & Quadrifoglio, F. (1987) *Nucleic Acids Res. 15*, 5803–5812.

Berman, H. M., Neidle, S., & Stodola, R. K. (1978) *Proc. Acad. Sci. U.S.A. 75*, 828–832.

Blackburn, M. (1990) in *Nucleic Acids in Chemistry and Biology* (Blackburn, M., & Gait, M., Eds.) Chapter 2, Oxford-IRL Press Ltd., Oxford.

Bresloff, J. L., & Crothers, D. M. (1981) *Biochemistry 20*, 3547–3553.

Broder, S. (1989) in *Concepts in Viral Pathogenesis III* (Notkins, A., & Oldstone, M., Eds.) pp 337–351, Springer-Verlag, Berlin.

Cantor, C. R., & Schimmel, P. R. (1980) in *Biophysical Chemistry*, W. H. Freeman and Co., San Francisco.

Chandrasekaran, S., Kusuma, S., Boykin, D. W., & Wilson, W. D. (1986) *Magn. Reson. Chem. 24*, 630–637.

Crothers, D. M. (1971) *Biopolymers 10*, 2147–2160.

Davidson, M. W., Griggs, B. G., Lopp, I. G., & Wilson, W. D. (1977) *Biochim. Biophys. Acta 479*, 378–390.

DeClercq, E., Ed. (1990) *Design of Anti-AIDS Drugs*, Vol. 14, Elsevier, Pharmacochemistry Library Series.

Dervan, P. B. (1986) *Science 232*, 464–471.

Haseltine, W. A. (1989) *J. Acquired Immune Defic. Syndr. 2*, 311–334.

Islam, S. A., & Neidle, S. (1984) *Acta Crystallogr. B40*, 424–429.

Jain, S. C., & Sobell, H. M. (1984a) *J. Biomol. Struct. Dyn. 1*, 1179–1194.

Jain, S. C., & Sobell, H. M. (1984b) *J. Biomol. Struct. Dyn. 1*, 1161–1177.

Jones, R. L., Lanier, A. C., Keel, R. A., & Wilson, W. D. (1980) *Nucleic Acids Res. 8*, 1613–1624.

Kapuscinski, J., & Szer, W. (1979) *Nucleic Acids Res. 6*, 3519–3534.

Kopka, M. L., Pjura, P., Yoon, C., Goodsell, D., & Dickerson, R. E. (1985a) in *Structure and Motion: Membranes, Nucleic Acids an Proteins* (Clementi, E., Corongiu, G., Sarma, M. H., & Sarma, R., Eds.) pp 461–483, Adenine Press, New York.

Kopka, M. L., Yoon, C., Goodsell, D., Pjura, P., & Dickerson, R. E. (1985b) *Proc. Natl. Acad. Sci. U.S.A. 82*, 1376–1380.

Kopka, M. L., Yoon, C., Goodsell, D., Pjura, P., & Dickerson, R. E. (1985c) *J. Mol. Biol. 183*, 553–563.

Krugh, T. R., & Nuss, M. E. (1979) in *Biological Applications of Magnetic Resonance* (Schulman, R. G., Ed.) Chapter 3, Academic Press, New York.

Kubista, M., Akerman, B., & Norden, B. (1987) *Biochemistry 26*, 4545–4553.

Larsen, T. A., Goodsell, D. S., Cascio, D., Grzeskowiak, K., & Dickerson, R. E. (1989) *J. Biomol. Struct. Dyn. 7*, 477–491.

Leroy, J. L., Broseta, D., & Gueron, M. (1985) *J. Mol. Biol. 184*, 165–178.

Lohman, T. M. (1985) *CRC Crit. Rev. Biochem. 19*, 191–235.

Lohman, T. M., DeHaseth, P. L., & Record, M. T. (1978) *Biophys. Chem. 8*, 281–294.

Macgregor, R. B., Clegg, R. M., & Jovin, T. M. (1987) *Biochemistry 26*, 4008–4016.

Manzini, G., Barvellona, M. L., Avitabile, M., & Quadrifoglio, F. (1983) *Nucleic Acids Res. 11*, 8861–8876.

Manzini, G., Xodo, L., Barcellona, M. L., & Quadrifoglio, F. (1985) *Nucleic Acids Res. 13*, 8955–8967.

Mitsuya, H., Yarchoan, R., & Broder, S. (1990) *Science 249*, 1533–1544.

Neidle, S. (1989) in *Landolt-Bornstein, Vol. VII/1b, Nucleic Acids* (Saenger, W., Ed.) pp 247–276, Spring-Verlag, Berlin, Heidelberg.

Neidle, S., & Abraham, Z. (1984) *CRC Crit. Rev. Biochem. 17*, 73–121.

Nelson, J. W., & Tinoco, I. Jr. (1984) *Biopolymers 23*, 213–233.

Patel, D. J. (1979) *Acc. Chem. Res. 12*, 118–125.

Portugal, J., & Waring, M. J. (1988) *Biochim. Biophys. Acta 949*, 158–168.

Pullman, A., & Pullman, B. (1981) *Q. Rev. Biophys. 14*, 189–380.

Rycyna, R. E. (1986) A conformational investigation of ultraviolet light-induced distortion in thymine and uracil model nucleic acids using nuclear magnetic resonance spectroscopy, Ph.D. Thesis, pp 242–248, State University of New York at Buffalo.

Saenger, W. (1984) in *Principles of Nucleic Acid Structure*, Springer-Verlag, New York.

Shieh, H.-S., Berman, H. M., Dabrow, M., & Neidle, S. (1980) *Nucleic Acids Res. 8*, 85–97.

Strekowski, L., Strekowska A., Watson, R. A., Tanious, F. A., Nguyen, L. J., & Wilson, W. D. (1987) *J. Med. Chem. 30*, 1415–1420.

Tanious, F. A., Yen, S. F., & Wilson, W. D. (1991) *Biochemistry 30*, 1813–1819.

Veal, J. M., & Wilson, W. D. (1991) *J. Biomol. Struct. Dyn. 8*, 1119–1145.

Waring, M. J. (1981) in *The Molecular Basis of Antibiotic Action* (Gale, E. F., Cundiffe, E., Reynolds, P. E., Richmond, M. H., & Waring, M. J., Eds.) 2nd ed., p 287, Wiley, New York.

Weiner, S. J., Kollman, P. A., Nguyen, D. T., & Case, D. A. (1986) *J. Comput. Chem. 7*, 230–252.

Wilson, W. D. (1990) in *Nucleic Acids in Chemistry and Biology* (Blackburn, M., & Gait, M., Eds.) Chapter 8, Oxford-IRL Press Ltd., Oxford.

Wilson, W. D., & Lopp, I. G. (1979) *Biopolymers 18*, 3025–3041.

Wilson, W. D., & Jones, R. L. (1981) *Adv. Pharmacol. Chemother. 18*, 177–222.

Wilson, W. D., Krishnamoorthy, C. R., Wang, Y. H., & Smith, J. C. (1985a) *Biopolymers 24*, 1941–1961.

Wilson, W. D., Wang, Y. H., Krishnamoorthy, C. R., & Smith, J. C. (1985b) *Biochemistry 24*, 3991–3999.

Wilson, W. D., Wang, Y. H., Kusuma, S., Chandrasekaran, S., Yang, N. C., & Boykin, D. W. (1985c) *J. Am. Chem. Soc. 107*, 4989–4995.

Wilson, W. D., Wang, Y. H., Krishnamoorthy, C. R., & Smith, J. C. (1986) *Chem.-Biol. Interact. 58*, 41-57.

Wilson, W. D., Strekowski, L., Tanious, F. A., Watson, R. A., Mokrosz, J. L., Strekowska, A., Webster, G. D., & Neidle, S. (1988) *J. Am. Chem. Soc. 110*, 8292–8299.

Wilson, W. D., Tanious, F. A., Watson, R. A., Barton, H. J., Strekowska, A., Harden, D. A., & Strekowski, L. (1989a) *Biochemistry 28*, 1984–1992.

Wilson, W. D., Tanious, F. A., Barton, H. J., Strekowski, L., Boykin, D. W., & Jones, R. L. (1989b) *J. Am. Chem. Soc. 111*, 5008–5010.

Wilson, W. D., Tanious, F. A., Barton, H. J., Wydra, R. I., Jones, R. L., Boykin, D. W. & Strekowski, L. (1990a) *Anti-Cancer Drug Des. 5*, 31–42.

Wilson, W. D., Tanious, F. A., Barton, H. J., Joens, R. L. Fox, K., Wydra, R. L., & Strekowski, L. (1990b) *Biochemistry 29*, 8452–8461.

Wilson, W. D., Li, Y., & Veal, J. M. (1992) in *Advances in DNA Sequence Specific Agents* (Hurley, L., Ed.) JAI Press, Greenwich, CT (in press).

Zimmer, C., & Wahnert, U. (1986) *Prog. Biophys. Mol. Biol. 47*, 31–112.